

Finite Volume Solution of the Fully Non-linear Weakly Dispersive Serre Equations[☆]

C. Zoppou^{a,*}, S. G. Roberts^a

^a*Department of Mathematics, Mathematical Sciences Institute, Australian National University, Canberra, ACT 0200, Australia*

Abstract

We validate a numerical approach for solving the one-dimensional non-linear weakly dispersive Serre equations. Although, the Serre equations describe an evolution-type behaviour, they are neither hyperbolic or parabolic. By introducing a new conserved variable the Serre equations can be written in conservation law form and numerical techniques for solving hyperbolic and elliptic equations are used to solve the Serre equations. We demonstrate how this is achieved and that it is straightforward to express other dispersion-type equations in this form. The hyperbolic system of equations are solved using the finite volume method and the auxiliary elliptic equations using finite differences. This approach allows us to accurately solve smooth and problems with steep gradients. The second-order numerical scheme is validated by choosing laboratory experimental data that involved dispersive waves produced by abrupt changes in the flow. It is shown to be accurate, simple to implement and stable for a range of problems including flows with steep gradients.

Keywords: dispersive waves, conservation laws, Serre equation, finite volume
2010 MSC: 76B15, 35L65, 65M08

1. Introduction

Rapidly-varying free surface flows are characterized by large surface gradients. These gradients produce vertical accelerations of fluid particles and a non-hydrostatic pressure distribution. If non-hydrostatic pressure distribution is assumed, one arrives at a system of equations that contain dispersive terms. Systems of equations that contain non-linear and dispersive terms are known as Boussinesq-type equations. There is however, no unique Boussinesq-type equation. Different derivation approaches and the order of accuracy of the terms retained in the derivation results in a variety of equations with different dispersion characteristics[1].

The validity of the various equation systems is still being debated. However, all require that the water depth $h_0 \ll L \sim 1/k$ is much smaller than the horizontal wave length, L , and k is

[☆]The work undertaken by the first author was supported financially by an Australian National University Postgraduate Research Award

*Corresponding author

Email addresses: Christopher.Zoppou@anu.edu.au (C. Zoppou), Stephen.Roberts@anu.edu.au (S. G. Roberts)

the wave number. The range of validity of these equations is dependent on the non-linearity parameter, $\epsilon = a/h_0$, where a is a typical wave amplitude. The Boussinesq wave theory requires the shallowness, $\sigma = h_0^2/L^2 \sim \epsilon \ll 1$.

In contrast to some Boussinesq-type equations, which rely on small amplitude theory, the fully non-linear and weakly dispersive Serre equations can be derived directly from the free surface incompressible Euler equations. In the literature the Serre equations are also known as the Green-Naghdi equations. There is no restriction on ϵ for the Serre equations[3] therefore, the Serre equations are applicable up to a wave breaking where $\epsilon \sim O(1)$ [4]. Bonneton *et al.*[5, 6] consider the weakly dispersive, fully non-linear Serre equations as the most appropriate system to model dispersive waves at the shoreline. If all the dispersion equations are ignored the equations revert to the non-linear hyperbolic shallow water wave equations.

Finite-difference schemes have been the most popular method for solving non-linear dispersive equations[7–10]. Finite-element techniques[11, 12][13] and spectral methods[14, 15] have also been employed. More recently, the finite volume method[2, 16–21] has become popular.

In many instances operator splitting techniques have been employed where standard shock capturing techniques are used to solve the shallow water wave equations and an implicit or semi-implicit finite difference scheme is used to solve the stiff source term, which contain the dispersive terms [2, 6, 17, 18, 21, 22]. The implication of using these approaches is that the problem should be smooth.

A major difficulty with solving Boussinesq-type and the Serre equations, it that the dispersive terms contain a mix spatial and temporal derivative term which is difficult to handle numerically. The mix derivative dispersive term can be written as a combination of temporal and spatial derivative terms so that the Serre equations can be expressed in conservation law form, with the water depth and a new quantity as conservative variables. The new formulation of the Serre equations allow the use of standard techniques for solving hyperbolic conservation laws to be applied to the solution of the Serre equations even though the Serre equations are neither hyperbolic or parabolic.

The approach used to transform the Serre equation in conservation law form is also applicable to other dispersion type equations. The numerical approach is validated using laboratory data. This is the first reported validation of this approach

A second-order finite volume technique is proposed for the solution of the fully non-linear and weakly dispersive Serre equations without the need for iteration or operator splitting. Second-order finite difference scheme is used to solve the elliptic equations for the remaining primitive variable, the fluid velocity. Le Mètayer *et al.*[23] used this approach in their highly diffusive first-order solution to the Serre equations.

There are very few examples in the literature validating models for solving dispersive equations which contain flows with steep gradients. Generally, smooth problems are chosen. For example, a wave train over a trapezoidal shoal is a standard validation test for numerical models based on the Boussinesq-type wave models, see for example Panda *et al.*[24] and Li *et al.*[13]. Shoaling solitary wave up a beach[5] [13] and reflection of a solitary wave from a vertical wall[24] [5] are other examples used to validate these models. Since our modelling approach was developed to handle both smooth and problems with steep gradients, we validate our modelling approach by specifically choosing laboratory data that involves steep gradients in the flow which produce dispersive waves. However, unlike the work of Le Mètayer *et al.*[23], we have provided on of the first attempts at validated a second-order scheme using laboratory data that involved dispersive waves produced by abrupt changes in the flow.

In the first part of this article the important features of the derivation of the standard Serre

equations in non-conservative and conservative form from the Euler equations is provided. In Section 2 the Serre equations are written in conservation law form by introducing a new conserved quantity and the properties of the linearized form of the Serre equation are examined. The second-order finite volume implementation of the proposed scheme is described in detail in Section 3. In Section 4, the numerical scheme is validated using an analytical solution and laboratory flume data. Finally, the performance of the numerical schemes is discussed in Section 5.

2. Serre Equations

For an inviscid incompressible fluid with constant density, ρ the conservation of mass and momentum are given by the Euler equations

$$\nabla \cdot \mathbf{u} = 0, \quad (1a)$$

and

$$\rho \frac{D\mathbf{u}}{Dt} = -\nabla p + \rho \mathbf{g} \quad (1b)$$

in two planar dimensions, $\mathbf{x} = (x, z)$, for a fluid particle at depth $\xi = z - h - z_b$ below the water surface, see Figure 1 there the water depth is $h(x, t)$ and $z_b(x)$ is the bed elevation. The fluid particle is subject to the pressure, $p(\mathbf{x}, t)$ and gravitational acceleration, $\mathbf{g} = (0, g)^T$ and has a velocity $\mathbf{u} = (u(\mathbf{x}, t), v(\mathbf{x}, t))$, where $u(\mathbf{x}, t)$ is the velocity in the x -coordinate and $v(\mathbf{x}, t)$ is the velocity in the z -coordinate and t is time. In addition to the above equations, a number of

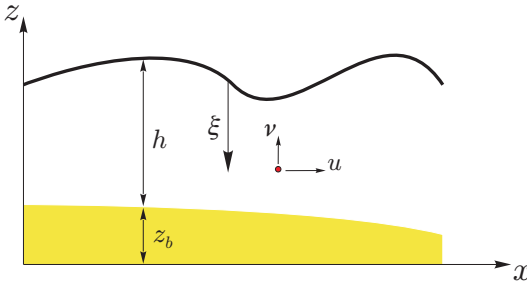


Figure 1: The notation used for one-dimensional flow governed by the Serre equation.

boundary conditions must be satisfied. These are;

- (a) the kinematic condition at the free surface ($z = h + z_b$),

$$v|_{h+z_b} = \frac{\partial h}{\partial t} + u \frac{\partial(h + z_b)}{\partial x} \quad (2a)$$

- (b) the kinematic condition at the bed ($z = z_b$)

$$v|_{z_b} = u \frac{\partial z_b}{\partial x} \quad (2b)$$

(c) the dynamic condition at the surface ($z = h + z_b$)

$$p(\xi = 0) = p_a. \quad (2c)$$

This is the atmospheric pressure at the water surface, usually taken to be zero gauge pressure at the free surface, $p_a = 0$.

The problem can be reduced from a two-dimensional to a one-dimensional problem by making an assumption about the velocity distribution of the horizontal velocity with water depth. The consequence of assuming the functional form of the horizontal velocity with water depth is a reduction in the dimension of the problem and the effect of the variation in the vertical velocity is incorporated by additional terms including a mixed spatial and temporal derivative term in the governing equations.

The choice of horizontal velocity variable, $u(x, t)$ to be used, results in a variety of equations with different forms and different dispersion characteristics[1, 10, 25–27]. It has been shown by Mei[28] and Nwogu[8] that the accuracy of linear dispersion characteristics is dependent on the choice of the velocity variable. The choice of velocity variable is not unique. In the derivation of the Serre equation, instead of using the velocity at a particular depth, the point velocity in the x -direction is assumed to be uniform over the water depth, so that $u(\mathbf{x}, t) = \bar{u}(x, t)$. where the depth-averaged velocity in the x -direction is given by

$$\bar{u} = \frac{1}{h} \int_{z_b}^{h+z_b} u(\mathbf{x}, t) d\zeta.$$

From (1a) it follows that the vertical velocity at any depth $z - z_b$ is given by

$$v|_z = -(z - z_b) \frac{\partial \bar{u}}{\partial x} \quad (3)$$

for a horizontal bed. The vertical velocity is a linear function of the water depth.

Integrating the point quantities in (1b) over the flow depth z_b to $h + z_b$, and satisfying (2) produces the one-dimensional equations

$$\frac{\partial h}{\partial t} + \frac{\partial(\bar{u}h)}{\partial x} = 0 \quad (4a)$$

and

$$\frac{\partial(\bar{u}h)}{\partial t} + \frac{\partial}{\partial x} \left(\bar{u}^2 h + \frac{gh^2}{2} \right) + \frac{\partial}{\partial x} \left[\frac{h^3}{3} \left(\frac{\partial \bar{u}}{\partial x} \frac{\partial \bar{u}}{\partial x} - \bar{u} \frac{\partial^2 \bar{u}}{\partial x^2} - \frac{\partial^2 \bar{u}}{\partial x \partial t} \right) \right] = 0 \quad (4b)$$

which are written in terms of the conservative variables, h and $\bar{u}h$ and the primitive variable \bar{u} . The continuity equation is exact and the momentum equation is an approximation??????.

The dispersive terms in the square parenthesis contain high order spatial derivative terms and a mixed derivative term. Some forms of the Boussinesq equation[29] ignore the mixed spatial and temporal derivative term and third-order space derivative terms.

The pressure at a depth ξ below the water surface, see Figure 1 is given by

$$p|_\xi = p_a + \rho g \xi + \frac{\rho}{2} \xi (2h - \xi) \left[\frac{\partial \bar{u}}{\partial x} \frac{\partial \bar{u}}{\partial x} - \bar{u} \frac{\partial^2 \bar{u}}{\partial x^2} - \frac{\partial^2 \bar{u}}{\partial x \partial t} \right]. \quad (5)$$

The dispersive term influences the pressure distribution, it is less than the hydrostatic pressure, $p(\xi) = \rho g \xi$ at the crest of a wave and greater than the hydrostatic pressure distribution at the troughs. Ignoring all the dispersive terms in (4b) results in the well known non-linear shallow water wave equations, where the pressure distribution is hydrostatic. Unlike the shallow water wave equations, which are hyperbolic for finite water depth, the Serre equations are neither hyperbolic or parabolic, although they also describe an evolution-type flows.

Equation (4) are known as the Serre equations[30–32] and unlike Boussinesq-type equations, they retain full non-linearity in the dispersive terms[33]. They have been derived by Serre[30], Su and Gardner[34] and Seabra-Santos *et al.*[31] and are equivalent to the depth averaged Green and Naghdi[35] equations. They are considered to be good approximations to the full Euler equations up to a wave breaking[5, 6].

2.1. Alternative Conservative Form of the Sere Equations

The flux term in the momentum equation, (4b) contains a mixed spatial and temporal derivative term which is difficult to treat numerically. It is possible to replace this term by a combination of spatial and temporal derivative terms by making the following observation

$$\frac{\partial^2}{\partial x \partial t} \left(\frac{h^3}{3} \frac{\partial \bar{u}}{\partial x} \right) = \frac{\partial}{\partial t} \left(h^2 \frac{\partial h}{\partial x} \frac{\partial \bar{u}}{\partial x} + \frac{h^3}{3} \frac{\partial^2 \bar{u}}{\partial x^2} \right) = \frac{\partial}{\partial x} \left(h^2 \frac{\partial h}{\partial t} \frac{\partial \bar{u}}{\partial x} + \frac{h^3}{3} \frac{\partial^2 \bar{u}}{\partial x \partial t} \right).$$

Rearranging and making use of the continuity equation, (4a) the momentum equation, (4b) becomes

$$\frac{\partial}{\partial t} \left(\bar{u}h - \frac{\partial}{\partial x} \left[h^3 \frac{\partial u}{\partial x} \right] \right) + \frac{\partial}{\partial x} \left(\bar{u}^2 h + \frac{gh^2}{2} - \bar{u} \frac{\partial}{\partial x} \left[\frac{h^3}{3} \frac{\partial \bar{u}}{\partial x} \right] - \frac{2h^3}{3} \frac{\partial \bar{u}}{\partial x} \frac{\partial \bar{u}}{\partial x} \right) = 0.$$

The momentum equation can be written in terms of a new conservative form as

$$\frac{\partial G}{\partial t} + \frac{\partial}{\partial x} \left(G \bar{u} + \frac{gh^2}{2} - \frac{2h^3}{3} \frac{\partial \bar{u}}{\partial x} \frac{\partial \bar{u}}{\partial x} \right) = 0 \quad (6)$$

where the new conserved quantity, G is given by

$$G = \bar{u}h - \frac{\partial}{\partial x} \left(\frac{h^3}{3} \frac{\partial \bar{u}}{\partial x} \right). \quad (7)$$

Given G and h , (7) can be solved using finite differences or finite elements for the primitive variable \bar{u} .

The temporal derivative in the momentum equation has been eliminated from the flux term. In contrast to (4), the flux term now only contains spatial derivatives. The quantity, G/h is known as irrotationality[32] or potential vorticity[14]. The quantity G is a new conserved variable that is admissible to the Serre equation. The Serre equations also admit the conservation of mass, momentum, energy and irrotationality[5, 32].

This approach can also be applied to other dispersive system of equations. For example, without justification, Barthélémy[4] added an additional dispersive term to (4b) so that the momentum equation becomes

$$\begin{aligned} \frac{\partial(\bar{u}h)}{\partial t} + \frac{\partial}{\partial x} \left(\bar{u}^2 h + \frac{gh^2}{2} \right) + \frac{\partial}{\partial x} \left[\frac{h^3}{3} \left(\frac{\partial \bar{u}}{\partial x} \frac{\partial \bar{u}}{\partial x} - \bar{u} \frac{\partial^2 \bar{u}}{\partial x^2} - \frac{\partial^2 \bar{u}}{\partial x \partial t} \right) \right] \\ + \beta h^3 \left[\frac{\partial^3 \bar{u}}{\partial x^2 \partial t} + g \frac{\partial^3 h}{\partial x^3} + \frac{\partial^2}{\partial x^2} \left(\bar{u} \frac{\partial \bar{u}}{\partial x} \right) \right] = 0 \end{aligned} \quad (8)$$

with β an arbitrary parameter used to improved the dispersion characteristics of (4b). Using the above approach, (8) can be written in conservation law form in terms of a new conservative variable as

$$\frac{\partial}{\partial t} \left(G + \beta h^3 \frac{\partial^2 \bar{u}}{\partial x^2} \right) + \frac{\partial}{\partial x} \left[\bar{u} \left(G + \beta h^3 \frac{\partial^2 \bar{u}}{\partial x^2} \right) + \frac{gh^2}{2} - \frac{2h^3}{3} \frac{\partial \bar{u}}{\partial x} \frac{\partial \bar{u}}{\partial x} \right] + \beta h^3 \left(g \frac{\partial^3 h}{\partial x^3} + 5 \frac{\partial \bar{u}}{\partial x} \frac{\partial^2 \bar{u}}{\partial x^2} \right) = 0$$

which does not contain a mixed spatial and temporal derivative source term and has the form of a conservation law with $G + \beta h^3 \partial^2 \bar{u} / \partial x^2$ as the conservative quantity. This equation can be treated numerically like a hyperbolic conservation law with a source term.

The alternative form of the Serre equations, (4a) and (6) can be written in vector form as

$$\frac{\partial \mathbf{v}}{\partial t} + \frac{\partial \mathbf{F}(\mathbf{v})}{\partial x} = 0. \quad (9a)$$

where the vector of state variables

$$\mathbf{v} = \begin{bmatrix} h \\ G \end{bmatrix}, \quad (9b)$$

and

$$\mathbf{F}(\mathbf{v}) = \begin{bmatrix} \bar{u}h \\ G\bar{u} + \frac{gh^2}{2} - \frac{2h^3}{3} \frac{\partial \bar{u}}{\partial x} \frac{\partial \bar{u}}{\partial x} \end{bmatrix}. \quad (9c)$$

Equation (9a) has the following numerical analogue.

$$\mathbf{v}_j^{n+1} = \mathbf{v}_j^n - \frac{\Delta t}{\Delta x} (\mathbf{F}_{j+1/2}^n - \mathbf{F}_{j-1/2}^n). \quad (10)$$

Since (9) is written in conservation law form, there are numerical techniques for solving this equation even if both conservative quantities are discontinuous. For the remaining primitive variable, \bar{u} , if the data G are square integrable in a rectangular domain, then from the regularity theorem of elliptic partial differential equations[36] $\bar{u} \in H^2$ in Sobolev space of square integrable second-derivatives. The primitive variable, \bar{u} will be smooth.

2.1.1. Properties of the Serre equations

The Serre equations are not hyperbolic or parabolic even though they describe evolution-type behaviour.

Some useful properties of the Serre equations, (4) or (9) can be obtained by applying the Fourier analysis to the linearized equations and observing the behaviour of a harmonic wave of the form

$$h(x, t) = A e^{i(kx - \omega t)} \quad \text{and} \quad u(x, t) = U e^{i(kx - \omega t)} \quad (11)$$

where A and U are unknown coefficients, ω is the frequency, k the wave number and $i = \sqrt{-1}$.

The linearized Serre equations are obtained by assuming that the solution of $\bar{u}(x, t)$ and $h(x, t)$ can be expressed as

$$h(x, t) = h_0(x, t) + \epsilon h_1(x, t) + \epsilon^2 h_2(x, t) + \dots \quad (12a)$$

and

$$\bar{u}(x, t) = u_0(x, t) + \epsilon u_1(x, t) + \epsilon^2 u_2(x, t) + \dots \quad (12b)$$

where ϵ is considered small and $u_0, u_1, \dots, h_0, h_1, \dots$ are to be determined.

Using (12), then the continuity equation, (4a) becomes, to terms of up to order ϵ

$$\frac{\partial h_1}{\partial t} + h_0 \frac{\partial u_1}{\partial x} + u_0 \frac{\partial h_1}{\partial x} = 0 \quad (13a)$$

and for the momentum equation, (4b)

$$\frac{\partial u_1}{\partial t} + g \frac{\partial h_1}{\partial x} + u_0 \frac{\partial u_1}{\partial x} - \frac{h_0^2}{3} \left(u_0 \frac{\partial^3 u_1}{\partial x^3} + \frac{\partial^3 u_1}{\partial x^2 \partial t} \right) = 0 \quad (13b)$$

which makes use of the linearized continuity equation.

Substituting (11), the linearized equations become

$$-A\omega + u_0 Ak + h_0 Uk = 0 \quad (14a)$$

and

$$-U\omega + gAk + u_0 Uk - \frac{1}{3}h_0^2 U\omega k^2 + \frac{1}{3}h_0^2 u_0 U k^3 = 0. \quad (14b)$$

For a non-trivial solution

$$\begin{vmatrix} -\omega + u_0 k & h_0 k \\ gk & -\omega + u_0 k - \frac{1}{3}h_0^2 \omega k^2 + \frac{1}{3}h_0^2 u_0 k^3 \end{vmatrix} = 0$$

or

$$\omega_{1,2} = u_0 k \pm k \sqrt{gh_0} \sqrt{\frac{3}{\mu^2 + 3}}$$

where $\mu = h_0 k$ is the frequency dispersion.

In this case the dispersive terms have no effect on u_0 , only on the celerity of a small disturbance. For non-dispersive waves, the phase velocity, $v_p = \text{Re}(\omega)/k$ is identical to the group velocity $v_g = d\text{Re}(\omega)/dk$. This is not the case for the Serre equation, where the phase speed is

$$v_p = u_0 \pm \sqrt{gh_0} \sqrt{\frac{3}{\mu^2 + 3}} \quad (15a)$$

and the group velocity is

$$v_g = u_0 \pm \sqrt{gh_0} \left(\sqrt{\frac{3}{\mu^2 + 3}} \mp \mu^2 \sqrt{\frac{3}{(\mu^2 + 3)^3}} \right) \neq v_p. \quad (15b)$$

Both are dependent on the wave number. Since the group speed is slower than the phase speed then the Serre equations describe dispersive waves.

3. Solving the Serre Equations Written in Conservation Law Form

A second-order finite volume method is used to solve the Serre equations, (9a). Second-order reconstruction is used to obtain the cell interface values, $\mathbf{v}_{j+1/2}^\pm$ from the cell average values. These are limited using the *generalized minmod* limiter[37]. The flux between the cells, $F_{j\pm 1/2}$ are estimated using the explicit upwind central approximate Riemann solver proposed by Kurganov *et al.*[38], where the intercell flux, $\mathbf{F}_{j+1/2}$ in (10) is given by

$$\mathbf{F}_{j-1/2} = \frac{a_{j+1/2}^+ \mathbf{f}_{j+1/2}^- - a_{j+1/2}^- \mathbf{f}_{j+1/2}^+}{a_{j+1/2}^+ - a_{j-1/2}^+} + \frac{a_{j+1/2}^+ a_{j+1/2}^-}{a_{j+1/2}^+ - a_{j-1/2}^-} (\mathbf{v}_{j+1/2}^+ - \mathbf{v}_{j+1/2}^-) \quad (16)$$

where the second component of the local fluxes, $\mathbf{f}_{j+1/2}^\pm$ are evaluated using first-order upwind differencing, so that

$$f_{j+1/2}^+ = (G\bar{u})_{j+1/2}^+ + \frac{gh_{j+1/2}^+}{2} - \frac{2h_{j+1/2}^+}{3\Delta x^2} (u_{j+3/2}^- - u_{j+1/2}^+)^2 \quad (17a)$$

$$f_{j+1/2}^- = (G\bar{u})_{j+1/2}^- + \frac{gh_{j+1/2}^-}{2} - \frac{2h_{j+1/2}^-}{3\Delta x^2} (u_{j+1/2}^- - u_{j-1/2}^+)^2. \quad (17b)$$

and the propagation speed, $a_{j+1/2}^\pm$ of a local shock at the cell interface are the only parameters required.

From (15) as the wave number approaches infinity, $k \rightarrow \infty$, $v_p \rightarrow v_g \rightarrow u_0 \pm \sqrt{gh_0}$, they are equal to the phase speed of shallow water waves where all wave components travel at the same speed, so that $v_p = v_g = u_0 \pm \sqrt{gh_0}$. When $k \rightarrow 0$, $v_p \rightarrow v_g \rightarrow u_0 \pm \sqrt{gh_0}$. Therefore, the phase speed for the Serre equations are bounded

$$u_0 - \sqrt{gh_0} \leq u_0 \pm \sqrt{gh_0} \sqrt{\frac{3}{\mu^2 + 3}} \leq u_0 + \sqrt{gh_0}$$

by the phase speed of the shallow water wave equations. We now have an estimate of the maximum and minimum shock speed required by the approximate Riemann solver.

Time integration is performed using a second-order Strong Stability Preserving (SSP) Runge-Kutta schemes[40, 42].

The second-order two-stage strong stability preserving Runge-Kutta scheme solution of the Serre equations involves the following steps

$$\begin{aligned} & \underbrace{\left[\begin{array}{c} h \\ G \end{array} \right]^n \xrightarrow{\mathcal{A}} \bar{u}^n}_{\textcircled{1}} \rightarrow \underbrace{\left[\begin{array}{c} h \\ G \end{array} \right]^{(1)}}_{\textcircled{2} \text{ First Euler Step}} = \underbrace{\left[\begin{array}{c} h \\ G \end{array} \right]^n - \Delta t \mathcal{L} \left[\begin{array}{c} h \\ G \end{array} \right]^n}_{\textcircled{3}} \\ & \underbrace{\left[\begin{array}{c} h \\ G \end{array} \right]^{(1)} \xrightarrow{\mathcal{A}} \bar{u}^{(1)}}_{\textcircled{4} \text{ Second Euler Step}} \rightarrow \underbrace{\left[\begin{array}{c} h \\ G \end{array} \right]^{(2)}}_{\textcircled{5} \text{ Average Step}} = \underbrace{\left[\begin{array}{c} h \\ G \end{array} \right]^{(1)} - \Delta t \mathcal{L} \left[\begin{array}{c} h \\ G \end{array} \right]^{(1)}}_{\textcircled{6}} \\ & \underbrace{\left[\begin{array}{c} h \\ G \end{array} \right]^{n+1}}_{\textcircled{5} \text{ Average Step}} = \frac{1}{2} \left[\begin{array}{c} h \\ G \end{array} \right]^n + \frac{1}{2} \left[\begin{array}{c} h \\ G \end{array} \right]^{(2)} \end{aligned}$$

where

$$\mathcal{L} = \frac{f_{j+1/2} - f_{j-1/2}}{\Delta x} \quad (18)$$

and $\Delta x = x_{j+1/2} - x_{j-1/2}$.

Step 1: Given h and G , the remaining primitive variable \bar{u} is obtained by solving the second-order elliptic equation, (19) using finite differences.

Step 2: Perform the reconstruction and solve the local Riemann problem to obtain the flux $F_{j\pm 1/2}$ of material across a cell interface. Evolve the solution using a first-order Euler time integration for the conserved quantities, h and G .

Steps 3 and 4: Repeat the process with the intermediate values and evolve using another first-order Euler step.

Step 5: The solution at the next time level is obtained by averaging the initial values and the values obtained from the second Euler step, which completes the second-order strong stability preserving Runge-Kutta time integration.

The operator $\bar{u} = \mathcal{A}[h, G]$ is the solution (7). Using second-order central differencing, then (7) can be written as

$$G_j = a_j \bar{u}_{j+1} + b_j \bar{u}_j + c_j \bar{u}_{j-1} \quad (19)$$

where

$$a_j = -\frac{h_j^2}{4\Delta x^2} (h_{j+1} - h_{j-1}) - \frac{h_j^3}{3\Delta x^2}$$

$$b_j = h_j + \frac{2h_j^3}{3\Delta x^2}$$

and

$$c_j = \frac{h_j^2}{4\Delta x^2} (h_{j+1} - h_{j-1}) - \frac{h_j^3}{3\Delta x^2}$$

which results in a tri-diagonal system of equations which can be solved efficiently using direct methods for \bar{u}_j given G_j and h_j for all the computational nodes $j = 1, \dots, m$.

With this approach h and G can be discontinuous, which is handled by the finite volume method and approximate Riemann solver efficiently. An attractive feature of this approach is that even if G is discontinuous, \bar{u} will always be smooth.

The resulting numerical scheme is theoretically $O(\Delta x^2, \Delta t^2)$ accurate. However, there is a restriction on the computational time-step that can be used in all explicit schemes. Stability is satisfied when the time step Δt satisfies the *Courant-Friedrichs-Lowy*, (CFL) criteria[43]

$$\Delta t < \frac{\Delta x}{2\max(|a_{j+1/2}^\pm|)} \quad \forall j???????$$

4. Numerical Simulations

Convergence rate of the proposed second-order solution of the Serre equations is determined using a known analytical solution to the Serre equations. Data from two laboratory experiments are used to validate the proposed model.

Comment: The equations do not contain a diffusion viscosity or bed friction which would dampen the simulated waves

4.1. Analytical Solution

The Serre equations, (4) has the following analytical solution[33](see, also Carter and Cienfuegos[32] and Chazel *et al.*[22])

$$h(x, t) = a_0 + a_1 \operatorname{sech}^2(\kappa(x - ct)) \quad (20a)$$

and

$$\bar{u}(x, t) = c \left(\frac{h(x, t) - a_0}{h(x, t)} \right) \quad (20b)$$

with

$$\kappa = \frac{\sqrt{3a_1}}{2a_0 \sqrt{a_0 + a_1}}$$

and

$$c = \sqrt{g(a_0 + a_1)}.$$

which is a solitary waves propagating at constant speed without deformation. There is a balance between non-linear and dispersive effects, resulting in waves that do no change with time. A numerical scheme must accurately model the equilibrium between amplitude and frequency dispersion in order to simulate the propagation of the wave profile at constant speed without deforming. Typical modelling problems involve the simulation of trailing edge dispersion waves which cause a reduction in wave height and celerity. This is a result from poorly balanced schemes and truncation errors in the numerical approximations.

The results from a numerical scheme are compared to the corresponding analytical solution by using the non-dimensionless L_1 norm for h as

$$L_1 = \frac{\sum_{j=1}^m |h_j - h(x_j)|}{\sum_{j=1}^m |h(x_j)|} \quad (22)$$

where, h_j is the simulated values of $h(x, t)$ at x_j , and $h(x_j)$ is the corresponding analytical solution. The L_1 norm is calculated using all the computational nodes, $j = 1, \dots, m$.

The prototypical example is a solitary wave predicted by (20) with, $a_0 = 10\text{m}$, $a_1 = 1.0\text{m}$ and $k = 1$. When $k = 1$ there is a solitary wave with wavelength $\lambda = \infty\text{m}$ and amplitude of 1.0m with a celerity, $c = 10.387974\text{m/s}$ and $\kappa = 0.026112/\text{m}$.

The boundary conditions imposed on the models are $h_0(x) = 10\text{m}$ and $u_0(x) = 0\text{m/s}$ at the upstream and downstream boundaries. Using these parameters, the initial soliton profile and velocity, the analytical and the simulated water depth and velocity at $t = 100\text{s}$ is shown in

Figure 2. The second-order scheme has not produced trailing waves in the solution, the soliton amplitude is accurately predicted and the soliton speed is captured correctly.

Performing the simulation for a range of Δx and keeping $Cr = 0.2$, the L_1 norm between the simulated and analytical solution was calculated for the water depth and fluid velocity. Plotting the $\log_{10} L_1$ against $\log_{10} \Delta x$ reveals that the proposed strategy for solving the Serre equations is second-order accurate, see Figure 3. It is shown to be second-order accurate.

Clearly, for the simulation of the smooth soliton problem, the scheme is capable of predicting the soliton speed and its amplitude as well.

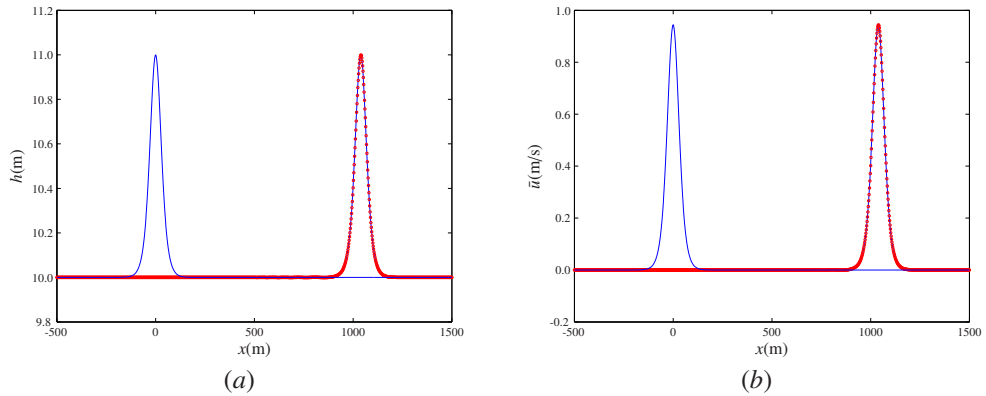


Figure 2: The progress of a initial solitary wave, given by (20) over a horizontal bed predicted by the second-order solution of (9) (\circ), where $\Delta x = 2\text{m}$, $\theta = 1.2$ and $Cr = 0.2$, at $t = 100\text{s}$ with the water depth, $h(x, t)$ shown in (a) and the velocity, $\bar{u}(x, t)$ in (b) plotted against the analytical solution (—).

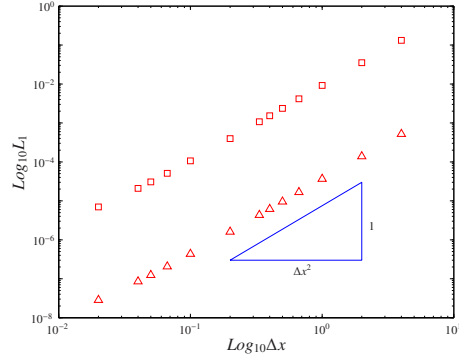


Figure 3: The L_1 convergence rate for the simulated water depth (\triangle) and velocity (\square) obtained from the second-order solution of (9) to the solitary wave example, given by (20).

4.2. Undular Bore

A surge propagation experiment conducted by Chanson[44] is used to validate the proposed modelling approach.

An undular bore was created in a large tilting flume at the Civil Engineering Department, University of Queensland. The channel is 0.5m wide, 12m in length and the undular bore was created in the horizontal flume, which has a smooth PVC bed and glass walls. A radial gate located at the downstream end of the flume, $x = 11.9\text{m}$ controls the water depth in the flume. The radial gate is used during the experiments to produce steady subcritical flow in the flume which remains constant for the duration of the experiment. Steady flow condition are established for 15 minutes prior to an experiment. Adjacent to the radial gate is a rapidly closing Tainter gate at, $x = 11.15\text{m}$ that spans the full width of the flume. An undular bore is generated by the rapid closure of the Tainter gate, which is estimated to take less than 0.2s, when water accumulates at the Tainter gate forming an upstream progressing undular bore. The experiment ceases when the bore reaches the intake structure to avoid any interference from wave reflection. Acoustic displacement meters, located at the flume centreline at; $x = 10.8, 8.0, 6.0, 5.0, 4.55, 4.0$ and 3.0m record the progress of the bore and dispersive waves with time. Data acquisition starts 30 seconds prior to the closure of the Tainter gate.

The boundary conditions imposed in all the models are; at the upstream boundary, $h(0, t) = 0.192\text{m}$ and $\bar{u}(0, t) = 0.199\text{m}^3/\text{s}$ and at the downstream Tainter gate, $h(11.15, t) = 0.22\text{m}$ and $\bar{u}(11.15, t) = 0\text{m}/\text{s}$. In all the simulations, $\Delta x = 0.01115\text{m}$ and $Cr = 0.2$ and $\theta = 1.2$ was used in the generalized minimod limiter.

The recorded water surface profile at the acoustic displacement meters over time are shown in Figure 4 along with the simulated water surface profile predicted by the second-order Serre equations solver.

Leakage has occurred beneath the Tainter gate. This can be seen from Figure 4(g) where the water depth decreases in time. This has also affected the recorded water level at $x = 8\text{m}$, shown in Figure 4(f). In all the other locations in the flume, the dispersive waves are symmetrical about the predicted water level. The results in Figure 4 show that the model accurately predicts the arrival of the bore. In addition, it has accurately predicted the amplitude of the dispersive waves which have a slightly longer wavelength than the actual dispersive waves.

4.3. Rectangular Initial Wave

Two frictionless horizontal flume experiments from Hammack and Segur[45], involving a negative amplitude rectangular wave are used to validate the proposed modelling approach.

In these experiments, a wave maker consists of a rectangular piston 61cm in length at the end of a wave tank spans the full width of the tank. The tank is 31.6m in length, 61cm deep and 39.4cm wide, horizontal with vertical sides and is constructed from glass. The piston moved monotonically from its initial position, which is flush with the tank bed to its final elevation. It can be displaced vertically up or down. The upstream wall of the wave tank adjacent to the wave maker is a plane of symmetry. The length of the piston, $b = 61\text{cm}$ represents the half-length of a hypothetical piston occupying the region $-b < x < b$. The symmetrical problem is simulated using the numerical schemes. A rectangular wave propagates following a sudden downward, $a_0 = h_1 - h_0$ movement of the piston, where h_0 is the water depth at the rectangular wave and h_1 is the initial water depth. Highly dispersive waves result from a discontinuous abrupt change in the initial flow conditions.

The water elevation is recorded at the fixed locations; $x/h_1 = 0, x/h_1 = 50, x/h_1 = 100, x/h_1 = 150$, and $x/h_1 = 200$, where $x/h_1 = 0$ is the downstream edge of the piston.

The upstream and downstream boundary conditions remain constant at; $h_1 = 10\text{cm}$ and $u_1 = 0\text{m}/\text{s}$. In all the numerical schemes $\Delta x = 0.0005\text{m}$, $Cr = 0.2$, $\Delta t = Cr\Delta x/\sqrt{0.1g}$ and $\theta = 1$

in the generalized limiter. The solution is terminated at $t = 50$ s for the two examples presented here where $a_0 = 3\text{cm}$ and $a_0 = 1\text{cm}$.

4.3.1. $a_0 = 3\text{cm}$

The dispersive waves for the $a_0 = 3\text{cm}$ laboratory experiment is shown in Figure 5. As the dispersive waves progress along the channel there seems to be a single wave train. The simulated results using the Serre equations solver are shown in Figure 5. There is excellent agreement between the simulated and observed results. The rarefaction wave, shock speed and the phase of the dispersive waves are faithfully reproduced by the numerical scheme. In addition, secondary wave trains are also reproduced by the numerical scheme, see for example Figure 5(c) at $t \sqrt{g/h_1} - x/h_1 \approx 110$. The amplitude of the dispersive waves, though are slightly overestimated by the numerical scheme.

The proposed modelling approach is capable of reproducing the dispersive waves associated with the rectangular wave. This is also confirmed in the following example.

4.3.2. $a_0 = 1\text{cm}$

In the second example, the amplitude of the rectangular wave is $a_0 = 1\text{cm}$ and the recorder dispersive waves are shown in Figure 6 along with the simulated results. There are two distinct wave trains, the amplitude of the second wave train is much smaller than the first. The model accurately predicts the phase speed and the amplitude of the dispersive waves for both wave trains.

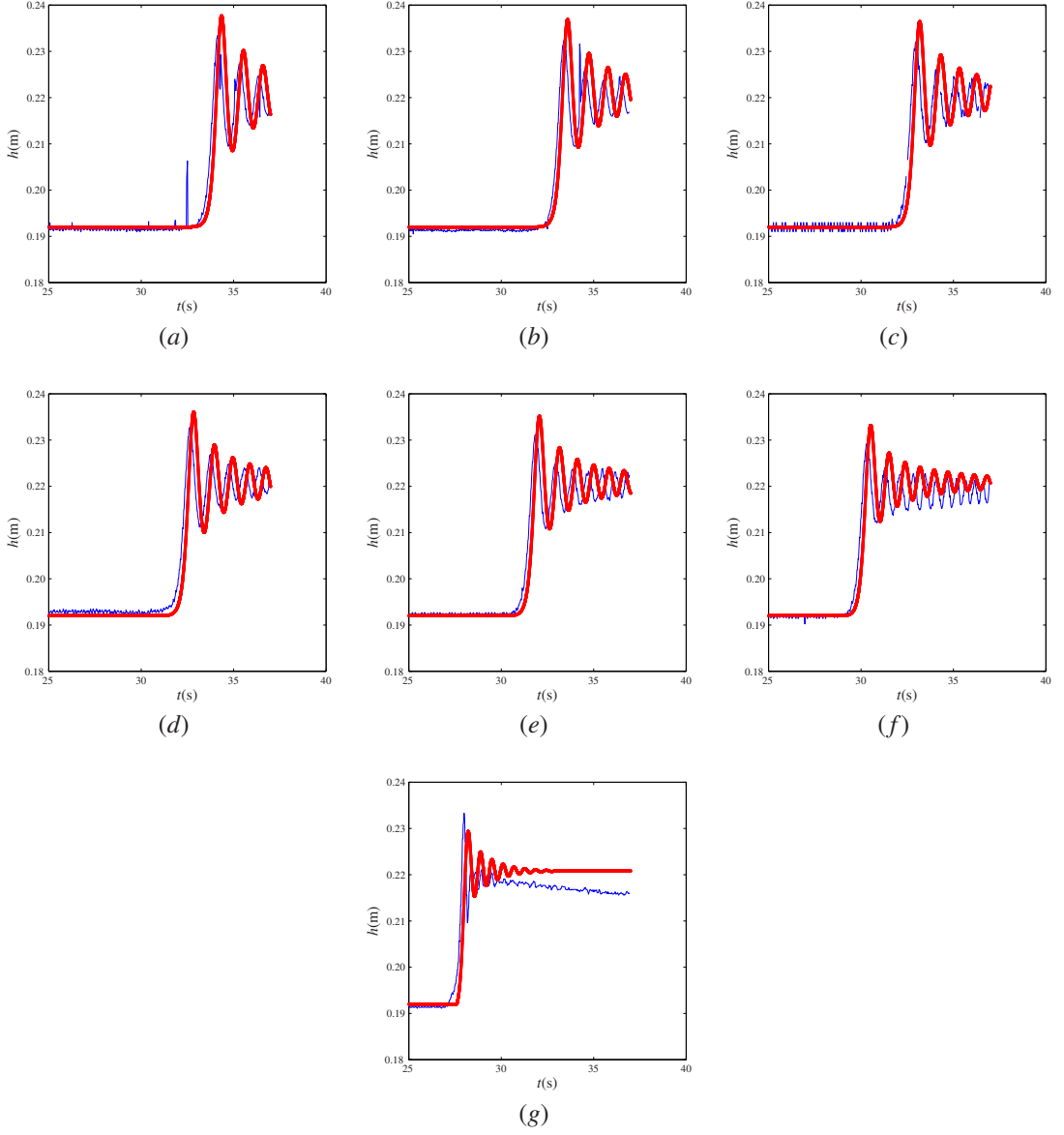


Figure 4: Measured (—) and simulated (\circ) water depth, $h(x, t)$ for the undular bore experiment in a frictionless rectangular channel using the second-order solution of the Serre equations with the simulated and measured results shown for (a) $x = 3\text{m}$, (b) $x = 4\text{m}$, (c) $x = 4.55\text{m}$, (d) $x = 5\text{m}$, (e) $x = 6\text{m}$, (f) $x = 8\text{m}$, and (g) $x = 10.8\text{m}$ using the generalized minimod limiter with $\theta = 1.2$, $\Delta x = 0.01115\text{m}$ and $Cr = 0.2$.

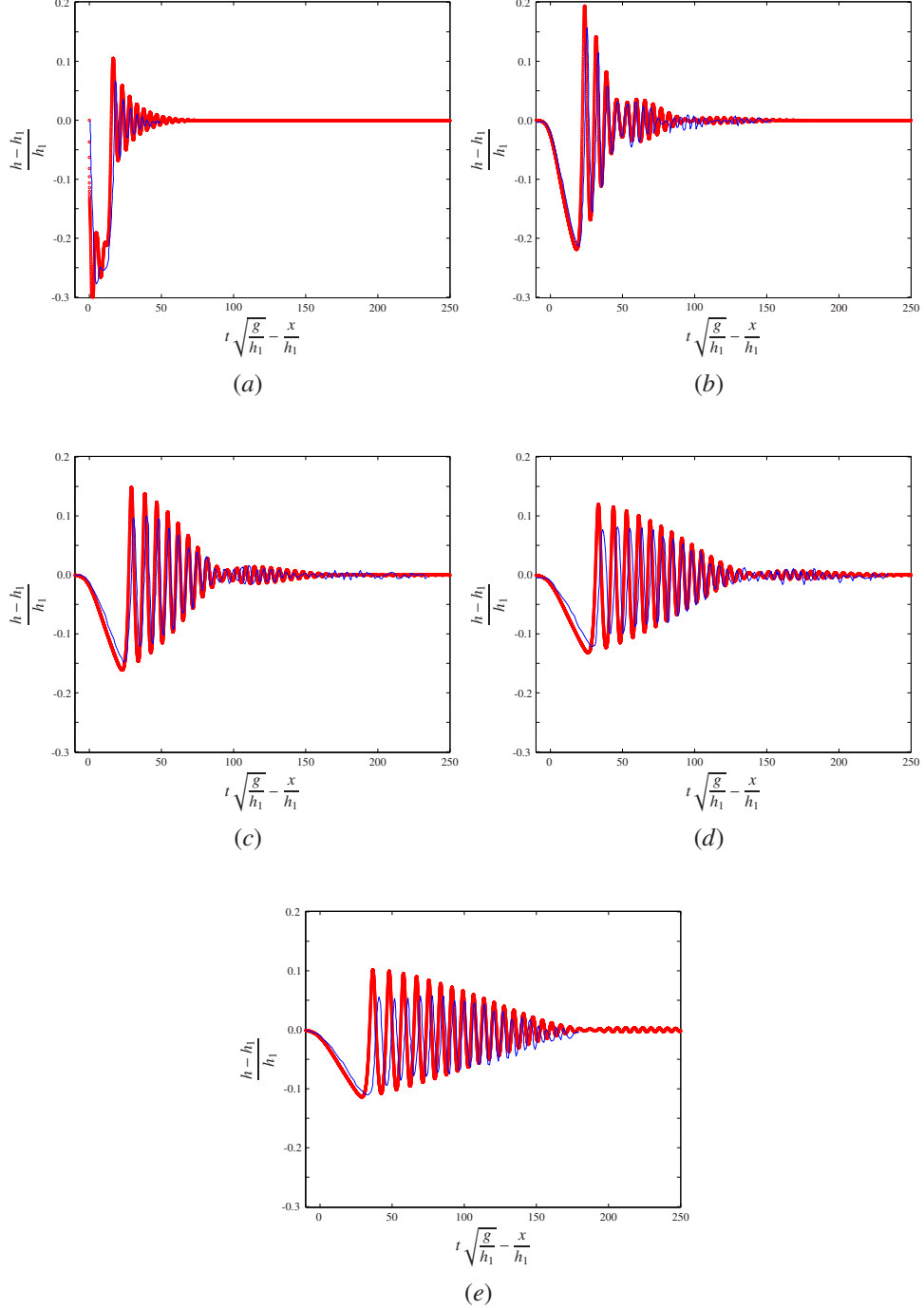


Figure 5: Measured (—) and simulated (\circ) water depth, $h(x, t)$ for the rectangular wave experiment in a frictionless rectangular channel, with $h_1 = 0.1\text{m}$, $u_1 = u_0 = 0\text{m/s}$ and $h_0 = 0.07\text{m}$ using second-order solution of the Serre equations with the simulated and measured results shown for the simulated and measured results shown for (a) $x/h_0 = 0$, (b) $x/h_0 = 50$, (c) $x/h_0 = 100$, (d) $x/h_0 = 150$, and (e) $x/h_0 = 200$ generalised minimod limiter with $\theta = 1.0$, $\Delta x = 0.005\text{m}$, $\Delta t = Cr\Delta x/\sqrt{gh_0}$ and $Cr = 0.2$.

5. Conclusions

We have managed to use techniques for solving conservation laws, to solve the Serre equations. This is achieved by replacing the mix spatial and temporal derivative dispersive term in the Serre equations with a combination of temporal and spatial terms. The Serre equations are re-written in conservation law form in terms of the new conserved quantity and evolved using a second-order finite volume scheme. The remaining primitive variable is obtained by solving a second-order elliptic equation. This approach can be applied to other dispersion equations and the use of standard techniques for solving conservation laws for the solution of the Serre equations to solve problems that are smooth or have steep gradients. Using an analytical solution and laboratory flume data, the proposed scheme is shown to be accurate, simple to implement and stable for a range of problems including flows with steep gradients. It accurately predicts the phase, arrival of the bore and dispersive waves and their amplitude.

Acknowledgements

Professor H. Chanson, Department of Civil Engineering, University of Queensland for providing the data for the undular bore and to Dr David George, Cascades Volcano Observatory, U.S. Geological Survey for providing the rectangular wave data.

- [1] P.A. Madsen, R. Murray, O.R. Sørensen, A new form of the Boussinesq equations with improved linear dispersion characteristics, *Coastal Engineering*, 15 (4) (1991) 371-388.
- [2] J.B. Shiach, C.G. Mingham, A temporally second-order accurate Godunov-type scheme for solving the extended Boussinesq equations, *Coastal Engineering*, 56 (1) (2009) 32-45.
- [3] Y.A. Li, A Shallow-Water Approximation to the Full Water Wave Problem, *Communications on Pure and Applied Mathematics*, 59 (9) (2006) 1255-1285.
- [4] E. Barthélémy, Non-linear shallow water theories for coastal waves, *Surveys in Geophysics*, 25 (3-4) (2004) 315-337.
- [5] P. Bonneton, F. Chazel, D. Lannes, F. Marche, M. Tissier, A splitting approach for the fully non-linear and weakly dispersive Green-Naghdi model, *Journal of Computational Physics*, 230 (4) (2011) 1479-1498.
- [6] P. Bonneton, E. Barthélémy, F. Chazel, R. Cienfuegos, D. Lannes, F. Marche, M. Tissier, Recent advances in Serre-Green Naghdi modelling for wave transformation, breaking and run-up processes, *European Journal of Mechanics B/Fluids*, 30 (6) (2011) 589-597.
- [7] A. Antunes do Carmo, F.J. Seabra-Santos A.B. Almeida, Numerical solution of the generalized Serre equations with the MacCormack finite-difference scheme, *International Journal for Numerical Methods in Fluids*, 16 (8) (1993) 725-738.
- [8] O. Nwogu, Alternative form of Boussinesq equations for near-shore wave propagation, *Journal of Waterway, Port, Coastal, and Ocean Engineering*, American Society of Civil Engineers, 119 (6) (1993) 618-638.
- [9] G.A. El, R.H.J. Grimshaw, N.F. Smyth, Asymptotic description of solitary wave trains in fully non-linear shallow-water theory, *Physica D*, 237 (19) (2008) 2423-2435.
- [10] S. Beji, K. Nadaoka, A formal derivation and numerical modelling of the improved Boussinesq equations for varying depth, *Ocean Engineering*, 23 (8) (1996) 691-704.
- [11] P. Avilez-Valente, F.J. Seabra-Santos, A high-order Petrov-Galerkin finite element method for the classical Boussinesq wave model, *International Journal for Numerical Methods in Fluids*, 59 (9) (2009) 969-1010.
- [12] D.E. Mitsotakis, Boussinesq systems in two-space dimensions over a variable bottom for the generation and propagation of tsunami waves, *Mathematics and Computers in Simulation*, 80 (4) (2009) 860-873.
- [13] M. Li, P. Guyenne, F. L, L. Xu. High order well-balanced CDG- methods for shallow water waves by a Green-Naghdi model, *Journal of Computational Physics*, 257 (2014) 169-192.
- [14] F. Dias, P. Milewski, On the fully-non-linear shallow-water generalized Serre equations, *Physics Letters A*, 374 (8) (2010) 1049-1053.
- [15] C. Eskilsson, S.J. Sherwin, A discontinuous spectral element model for Boussinesq-type equations, *Journal of Scientific Computing*, 17 (1-4) (2002) 143-152.
- [16] K.S. Erduran, S. Ilic, V. Kutija, Hybrid finite-volume finite-difference scheme for the solution of Boussinesq equations, *International Journal for Numerical Methods in Fluids*, 49 (11) (2005) 1213-1232.

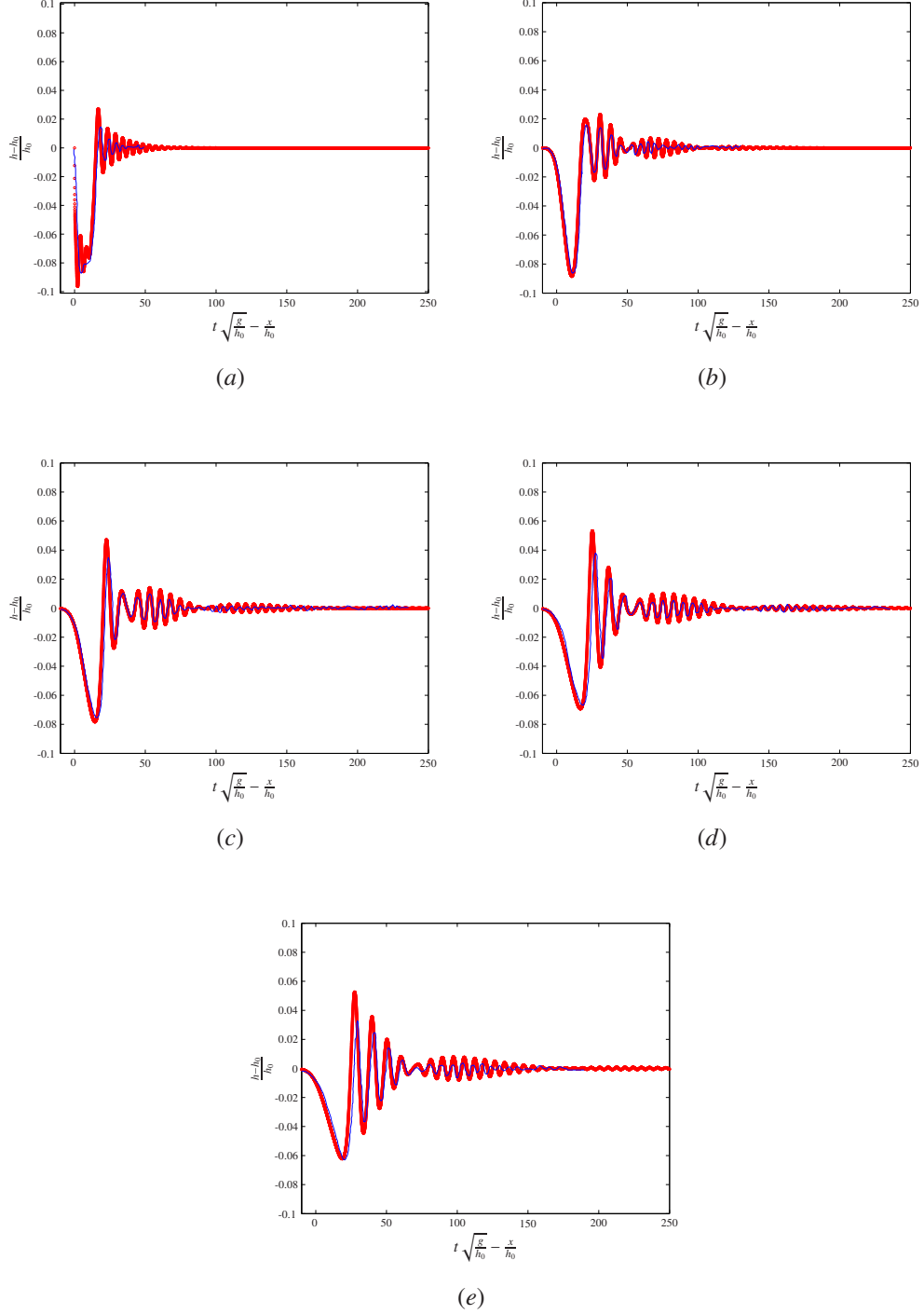


Figure 6: Measured and simulated water depth, h for the rectangular initial wave experiment in a frictionless channel, 50m in length, $L = 1.22\text{m}$, $h_0 = 0.09\text{m}$, $\bar{u}_1 = 0\text{m}^3/\text{s}$, $h_1 = 0.1\text{m}$ and $\bar{u}_0 = 0\text{m}/\text{s}$ using second-order solution of the Serre equations with the simulated and measured results shown for $x/h_1 = (a) 0, (b) 50, (c) 100, (d) 150$ and (e) 200 with $\Delta x = 0.01\text{m}$ and $Cr = 0.2$.

- [17] K.S. Erduran, Further application of hybrid solution to another form of Boussinesq equations and comparisons, International Journal for Numerical Methods in Fluids, 53 (5) (2007) 827-849.
- [18] S. Soares-Frazão, V. Guinot, A second-order semi-implicit hybrid scheme for one-dimensional Boussinesq-type waves in rectangular channels, International Journal for Numerical Methods in Fluids, 58 (3) (2008) 237-261.
- [19] M. Tonelli, M. Petti, Shock-capturing Boussinesq model for irregular wave propagation, Coastal Engineering, 61 (2012) 8-19.
- [20] V. Roeber, K.F. Cheung, M.H. Kobayashi,, Shock-capturing Boussinesq-type model for near shore wave processes, Coastal Engineering, 57 (4) (2010) 407-423.
- [21] M. Tonelli, M. Petti, Hybrid finite volume-finite difference scheme for 2DH improved Boussinesq equations, Coastal Engineering, 56 (5-6) (2009) 609-620.
- [22] F. Chazel, D. Lannes, F. Marche, Numerical simulation of strongly non-linear and dispersive waves using a Green-Naghdi model, Journal of Scientific Computing, 48 (1-3) (2011) 105-116.
- [23] O. Le. Métayer, S. Gavrilyuk, S. Hank, A numerical scheme for the Green-Naghdi model, Journal of Computational Physics, 229 (6) (2010) 2034-2045.
- [24] N. Panda, C. Dawson, Y. Zhang, A.B. Kennedy, J.J. Westerink, A.S. Donahue, Discontinuous Galerkin methods for solving Boussinesq-Green-Naghdi equations in resolving non-linear and dispersive surface water waves, Journal of Computational Physics, 273 (2014) 572-588.
- [25] P.A. Madsen, O.R. Sørensen,, A new form of Boussinesq equations with improved linear dispersion characteristics. Part II. A slowly-varying bathymetry, Coastal Engineering, 18 (3-4) (1992) 183-204.
- [26] G.B. Witting, A unified model for the evolution of non-linear water waves, Journal of Computational Physics, 56 (2) (1984) 203-236.
- [27] Z.L. Zou,, Higher order Boussinesq equations, Ocean Engineering, 26 (8) (1999) 767-792.
- [28] C.C. Mei, M. Stiassnie, D.K.K. Yue, Theory and Applications of Ocean Surface Waves Part 2 - Non-linear Aspects, Advanced Series on Ocean Engineering, Volume 23, World Scientific, Singapore, 2005.
- [29] D.R. Basco, Computation of rapidly varied, unsteady, free-surface flow, US Geological Survey, Water-Resources Investigations Report, 83-4284 (1987).
- [30] F. Serre, Contribution à l'étude des écoulements permanents et variables dans les canaux, La Houille Blanche, 6 (1953) 830-872.
- [31] F.J. Seabra-Santos, D.P. Renouard, A.M. Temperville, Numerical and experimental study of the transformation of a solitary wave over a shelf or isolated obstacle, Journal of Fluid Mechanics, 176 (1981) 117-134.
- [32] J.D. Carter, R. Cienfuegos, Solitary and cnoidal wave solutions of the Serre equations and their stability, European Journal of Mechanics B/Fluids, 30 (3) (2011) 259-268.
- [33] G.A. El, R.H.J. Grimshaw, N.F. Smyth, Unsteady undular bores in fully non-linear shallow-water theory, Physics of Fluids, 18 (2006), 027104.
- [34] C.H. Su, C.S. Gardner, Korteweg-de Vries equation and generalisations. III. Derivation of the Korteweg-de Vries equation and Burgers equation, Journal of Mathematical Physics, 10 (3) (1969) 536-539.
- [35] A.E. Green, P.M. Naghdi, A derivation of equations for wave propagation in water of variable depth, Journal of Fluid Mechanics, 78 (2) (1976) 237-246.
- [36] L.C. Evans, *Partial Differential Equations*, Graduate Studies in Mathematics, Volume 19, American Mathematical Society, New York, (1997).
- [37] B. van Leer, Towards the ultimate conservative difference scheme, V. A second-order sequel to Godunov's method, Journal of Computational Physics, 32 (1) (1979) 101-136.
- [38] A. Kurganov, S. Noelle, G. Petrova, Semidiscrete central-upwind schemes for hyperbolic conservation laws and Hamilton-Jacobi equations, Journal of Scientific Computing, Society for Industrial and Applied Mathematics, 23 (3) (2002) 707-740.
- [39] C. Zoppou, S. Roberts, Explicit schemes for dam-break simulations, Journal of Hydraulic Engineering, American Society of Civil Engineers, 129 (1) (2003) 11-34.
- [40] C.W. Shu, S. Osher, Efficient implementation of essentially non-oscillatory shock-capturing schemes, Journal of Computational Physics, 77 (2) (1988) 439-471.
- [41] S. Gottlieb, D.I. Ketcheson, C.W. Shu, High order strong stability preserving time discretizations, Journal of Scientific Computing, 38 (3) (2009) 251-289.
- [42] C.B. Macdonald, S. Gottlieb, S.J. Ruuth, A Numerical Study of Diagonally Split Runge-Kutta Methods for PDEs with Discontinuities, Journal of Scientific Computing, 36 (1) (2008) 89-112.
- [43] A. Harten, High resolution schemes for hyperbolic conservation laws, Journal of Computational Physics, 49 (3) (1983) 357-393.
- [44] H. Chanson, An experimental study of tidal bore propagation: The impact of bridge piers and channel constriction, School of Civil Engineering, The University of Queensland, Research Report CH74/09, 104p. (2009).
- [45] J.L. Hammack H. Segur, The Korteweg-de Vries equation and water waves. Part 3 . Oscillatory waves, Journal of Fluid Mechanics, 84 (2) (1978) 337-358.